World Academy of Science, Engineering and Technology
International Journal of Geological and Environmental Engineering
Vol:11, No:9, 2017

Sphere in Cube Grid Approach to Modelling of Shale Gas Production Using Non-Linear Flow Mechanisms

Dhruvit S. Berawala, Jann R. Ursin, Obrad Slijepcevic

Abstract**—**Shale gas is one of the most rapidly growing forms of natural gas. Unconventional natural gas deposits are difficult to characterize overall, but in general are often lower in resource concentration and dispersed over large areas. Moreover, gas is densely packed into the matrix through adsorption which accounts for large volume of gas reserves. Gas production from tight shale deposits are made possible by extensive and deep well fracturing which contacts large fractions of the formation. The conventional reservoir modelling and production forecasting methods, which rely on fluid-flow processes dominated by viscous forces, have proved to be very pessimistic and inaccurate. This paper presents a new approach to forecast shale gas production by detailed modeling of gas desorption, diffusion and non-linear flow mechanisms in combination with statistical representation of these processes. The representation of the model involves a cube as a porous media where free gas is present and a sphere (SiC: Sphere in Cube model) inside it where gas is adsorbed on to the kerogen or organic matter. Further, the sphere is considered consisting of many layers of adsorbed gas in an onion-like structure. With pressure decline, the gas desorbs first from the outer most layer of sphere causing decrease in its molecular concentration. The new available surface area and change in concentration triggers the diffusion of gas from kerogen. The process continues until all the gas present internally diffuses out of the kerogen, gets adsorbs onto available surface area and then desorbs into the nanopores and micro-fractures in the cube. Each SiC idealizes a gas pathway and is characterized by sphere diameter and length of the cube. The diameter allows to model gas storage, diffusion and desorption; the cube length takes into account the pathway for flow in nanopores and micro-fractures. Many of these representative but general cells of the reservoir are put together and linked to a well or hydraulic fracture. The paper quantitatively describes these processes as well as clarifies the geological conditions under which a successful shale gas production could be expected. A numerical model has been derived which is then compiled on FORTRAN to develop a simulator for the production of shale gas by considering the spheres as a source term in each of the grid blocks. By applying SiC to field data, we demonstrate that the model provides an effective way to quickly access gas production rates from shale formations. We also examine the effect of model input properties on gas production.

Keywords**—**Adsorption, diffusion, non-linear flow, shale gas production.

I. Introduction

FROM the advert of the modern oil and gas industry, petroleum geologists and engineers have followed a conventional route for exploration; look for hydrocarbon source rocks, find reservoir quality rocks where hydrocarbons can accumulate, identify a trapping mechanism and then drill a well. However, a revolution is taking place in the E&P industry. Rocks that in the past were of little interest, other than as potential source rocks, are today being actively pursued as potential reservoirs. When considering unconventional resource plays, the focus is on finding organic shale's [1]. They are sedimentary rocks that fall under the category of mudstones. These formations are composed of illite, smectite and kaolinite clay minerals. Black shales are the ones containing organic material that sometimes breaks down to form natural gas or oil.

Shale gas reservoirs differ from the conventional gas reservoirs by two important characteristics. Firstly, they have very low matrix permeability. Secondly, in some instances they contain organic-rick rocks where gas can also be adsorbed. Javadpour et al. [2] suggested different gas storage processes in gas shale namely; compressed free gas in nanoscale pores in the organic matter, and dissolved gas in the kerogenic material.

The gas in shale reservoirs is stored in three ways:

- Free gas in pores and fractures
- Adsorbed gas onto organic matter & clay minerals in the matrix
- Dissolved gas in oil & water

Shale gas is one of the most rapidly growing forms of natural gas. It will make a major contribution to future world gas production. These are the complex rocks characterized by heterogeneity in structure and composition in all scales. However, understandings and technologies needed for effective development of these resources are still lacking and as a result, we have low gas recovery. There have been numerous approaches to model the gas production from the reservoirs from advanced simulators to analytical solutions. Moreover, the extremely low permeability of shale reservoirs gives steady and continuous presence of pressure transient effects during well production. This long-term shale gas well performance characteristics are generally not well understood. This makes production forecasting a difficult and non-unique exercise. In this paper, we present a new methodology to explain the characteristics of well performance by modelling gas production using a unique sphere-in-cube grid approach.

Gas in shale reservoirs is present both in the naturally occurring micro fractures and adsorbed onto the surface of the shale grains. By storing gas in a dense, liquid-like adsorbed phase, the overall storage capacity of the rock is increased relative to if there were a free gas phase alone. Moreover, the release of this adsorbed phase is pressure dependent. As a reservoir is depleted, the adsorbed phase is freed, providing not just additional gas for production but helping to maintain

D. S. Berawala, J. R. Ursin and O. Slijepcevic are with the Department of Petroleum Engineering, University of Stavanger, Stavanger, 4036 Norway (e-mail: dhruvit.s.berawala@uis.no, jann-rune.ursin@uis.no, obradgas@gmail.com).

pressure (and perhaps open pore throats for fluid flow) as well. While adsorption allows for larger quantities of gas to be in place and possibly produced, factors such as desorption pressure, kinetics, and alteration of effective stresses makes it difficult to know if desorbed gas will contribute significantly to production [3].

Gas production from this tight shale deposits are made possible by hydraulically fracturing the wells to connect large fractions of the reservoir. Production of gas takes place by gas diffusion within the matrix and by Darcy type flow in the well-induced fractures.

II. Flow Model Description

A. Sphere-in-Cube Grid Flow Model Approach

In this work, we develop a flow model with a cell in the shape of a cube and a sphere inside it (Fig. 1). The gas is considered to be stored in natural fractures, pores and adsorbed onto kerogen/organic matter. When the production initiates, free gas from the natural fractures is produced first which is fed by matrix and matrix is then fed by adsorbed gas on kerogen or organic matter exposed inside the nanopores. Matrix here means both the organic matter or kerogen and the inorganic matter. However, the inorganic matter have much bigger pores and they are be classified as micro-fractures. These micro-fractures become active after hydraulically fracturing the formation. Thus, it is convenient to define pore space inside the organic matter as matrix and that of in the inorganic matter as micro-fractures.

For the ease of modelling, we assume all the kerogen bulk or organic matter to be located inside the sphere. Thus, the amount of adsorbed gas is present only inside the sphere as shown in Fig. 1. Moreover, the space outside of sphere and inside the cube is assumed to consists only inorganic matter with micro-fractures where free gas is stored. In actual reservoir, the organic matter is much more dispersed but this assumption is to efficiently model the gas production.

The sphere is further considered consisting of many layers in an onion-like structure. When the production initiates, free gas from the micro-fractures flows first to the well-induced fracture. With pressure decline below critical desorption pressure, the gas desorbs first from the outer most layer of sphere causing decrease in molecular concentration of gas. The new available surface area and change in concentration triggers the diffusion of gas from kerogen.

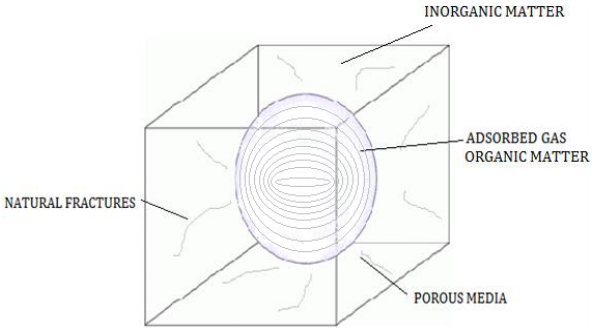

Fig. 1 A representation of sphere-in-cube grid block

The process continues to all the layers present internally until all the gas diffuses out of the kerogen, absorbs onto available surface area and desorbs into the micro-fractures in the cube. This shows the extent of gas transport in shale gas reservoirs. Langmuir's Isotherm [4] gives the amount of gas adsorbed onto the matrix.

Many of these representative but general cells are put together forming a layer of reservoir and linked to a well-induced fracture as shown in Fig. 2. The flow of gas is from one cell to another and then to the well through the well-induced fracture.

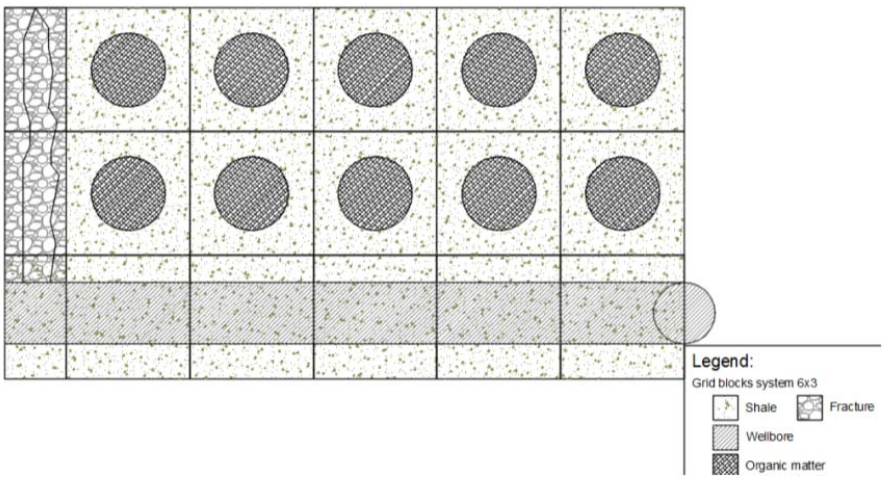

Fig. 2 Reservoir model representing the flow of shale gas from matrix to micro-fractures to well-induced fractures and to the horizontal well

B. List of Assumptions

- The gas flows from the matrix or micro-fracture to the well induced fracture and then to the horizontal well bore. No gas flows directly from the matrix to the well bore.
- A single fracture is surrounded by porous matrix. The flow in the matrix occurs in the horizontal x-direction only.
- The flow in well induced fracture occurs in both x-z

direction.

- Non-linear flow using Forchheimer's equation [5] is used to model flow of gas within matrix and micro-fracture.
- Linear flow using Darcy's equation is used for the flow of gas in well induced fracture.
- Desorption of gas is pressure dependent which is defined by Langmuir's isotherm [4].
- Free gas and desorbed gas attains equilibrium immediately once the pressure in the reservoir reaches critical desorption pressure [3].
- Single phase flow of gas in considered, i.e., it is assumed that the reservoir is a dry-gas reservoir or that it contains insignificant amount of water.
- The composition of free gas and desorb gas is same and there is no difference in the specific gravities of the two gases.

III. Flow Mechanisms

A. Diffusion of Gas in Sphere

Solute diffusion into porous soil aggregates and into litho-fragments in sediments and aquifer materials in the sorptive uptake and desorption mode may be described with Fick's second law in spherical coordinates (Fig. 3):

$$\frac{\partial C}{\partial t} = D_a \left[\frac{\partial^2 C}{\partial r^2} + \frac{2}{r}\frac{\partial C}{\partial r}\right] \quad (1)$$

where C, t and r denote concentration, time and the radial distance from the centre of the sphere [6].

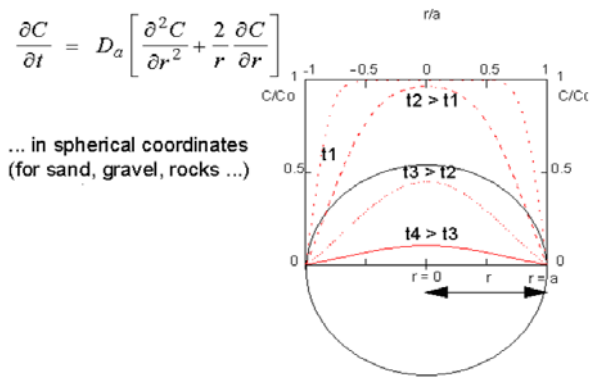

Fig. 3 Diffusion out of sphere: concentration profiles after times t1-t4. a is the radius of the sphere and r is the radial distance (coordinated from the centre) [6]

The equation for 1D diffusive flow through mineral matrix for a spherical shape [7] is expressed as:

$$\frac{\partial(\emptyset_m C_{i,m})}{\partial t} = \frac{1}{r^2}\frac{\partial}{\partial r}\left(r^2 D_{e,m}\frac{\partial C_{i,m}}{\partial r}\right), \quad (2)$$

where $\emptyset_m$ is the porosity of the matrix, $C_{i,m}$ is the concentration within matrix, and $D_{e,m}$ is the effective diffusion coefficient of the matrix. Initially, the gas diffusion rate will be zero as both the kerogen bulk and matrix (nanopores) are at initial reservoir pressure. However, in the mathematical model here, we assume that desorption of gas is only pressure dependent and we neglect the gas transport process of desorbed gas through diffusion. This indicates that with pressure changes, the adsorbed gas will reach balance with free gas in the micro-fractures immediately. This assumption is acceptable because of two considerations:

i. Firstly, the rate of molecular diffusion and mass transport differ a large amount from each other. In fact, the rate of molecular diffusion is much higher than that of mass transport.
ii. Secondly, the pressure in shale gas reservoirs changes very slowly due to low matrix permeability or low flow rate. So as the pressure changes, the time needed to reach a new balance between gases adsorbed and free gas is so short that it can be neglected [3], [8].

B. Adsorption/Desorption in Shale Gas Reservoirs

In this research, Langmuir's isotherm [4] is used to define the relationship of pressure and gas storage capacity of the reservoir rock. Langmuir's isotherm is mathematically defined as:

$$V_E = V_L \frac{P}{P + P_L} \quad (3)$$

where, V_E - Gas content or Langmuir's volume (scf/ton) (standard volume adsorbed per unit rock mass). V_L – Maximum amount of adsorbed gas, function of the organic richness, TOC (scf/ton); P – Reservoir gas pressure (psi); P_L – Langmuir's pressure (psi), pressure at which 50% pf the gas is desorbed.

Gas is assumed to be adsorbed on the internal surface of nanopores inside kerogen. It is supposed to first desorb from the surface of the nanopores into the matrix pores, which then feeds the fracture. Though adsorbed gas is in contact with matrix pressure, initially it may be under saturated and therefore at equilibrium with a lower pressure as observed in many CBM reservoirs [9]. It is only when the matrix pressure reaches this lower pressure, termed as critical desorption pressure ($P_{critdes}$) that the adsorbed gas starts desorbing [10].

From (3), adsorbed volume V_{des} (scf) can be written in terms of bulk volume V_b (ft^3) and rock density ρ_R (lbm/ft^3) as:

$$V_{des} = V_L V_b \rho_R \frac{P}{(P+P_L)} \quad (4)$$

Gas rate (scf/sec) from desorption into total matrix pore space can then be found by differentiating (4) with respect to time. We get,

$$\dot{Q}_{des} = -\frac{\partial V_{des}}{\partial t} = -V_L V_b \rho_R \frac{P_L}{(P+P_L)^2}\frac{\partial P}{\partial t} \quad (5)$$

$$\dot{m}_{des} = -\frac{\partial V_{des}}{\partial t} = -V_L V_b \rho_R \rho_{ntp} \frac{P_L}{(P+P_L)^2}\frac{\partial P}{\partial t} \quad (6)$$

Equation (5) gives the volumetric rate (scf/sec) whereas (6) gives us the mass rate (kg/sec) of gas desorbed.

The adsorbed gas at any stage of depletion has its own equilibrium pressure (*Pad*) which is different from the matrix

pressure. Once matrix pressure reaches critical desorption pressure and desorption commences, this equilibrium pressure (P_{ad}) remains higher than the matrix pressure due to a time lag caused by sorption time and possibly phase behaviour effects of adsorbed gas [3], [11]. This sorption time decreases the ease of desorption and the lag between the adsorbed gas and matrix pressure [10]. However, for simplicity, this effect has been neglected in the model presented, i.e., sorption time approaches zero and the system will tend to attain instant equilibrium between adsorbed phase and matrix. Gas desorption rate is considered to depend only upon the matrix pressure. The lower the matrix pressure, the higher the higher the rate of desorption.

C. Non-Darcy Flow

Tight/shale gas reservoirs contain a wide distribution of pore sizes, including in some cases nano-pores [12]. Therefore, the mean-free path of gas molecules may be comparable to or larger than the average effective rock pore throat radius causing the gas molecules to slip along pore surfaces. This results in slippage non-Darcy flow [13].

Forchheimer [5] investigated fluid flow through porous media in the high velocity regime. As flow velocity increases, the inertial effects dominating the flow were observed. The mathematical equation that is used to describe non-linear flow mechanism is given as:

$$-\frac{d^2P}{dx^2} = \frac{\mu}{K}\frac{dv}{dx} + 2\beta\rho v\frac{dv}{dx} \tag{7}$$

where μ is fluid (gas) viscosity (cP); K is permeability (mD); β is non-Darcy coefficient; ρ is density of fluid (gas) in (kg/m^3); v is fluid (gas) velocity (m/s).

IV. Mass Balance Equations

A. Geometry of Fracture-Matrix System

Consider a system in x-z plane consisting of single fracture perpendicular to horizontal well as shown in Fig. 2. The system is divided into various grids with matrix zone and fracture zone. Matrix zone consists of sphere where adsorbed gas is stored whereas only free gas is present in the well-induced fracture. The fracture and matrix grid dimensions are given as input parameters.

The continuity equation for one-dimensional flow of mass along the x-axis and out of a volume element ΔV (ft^3) of length ΔX (ft.) with porosity Ø and the cross-sectional area A (ft^2), in terms of gas density ρ_g and gas velocity u_g is:

$$\frac{\partial}{\partial x}(\rho_g u_g) = -\frac{\partial}{\partial t}(\emptyset\rho_g) \tag{8}$$

$$\text{Or} \quad \rho_g\frac{du_g}{dx} + u_g\frac{d\rho_g}{dx} = -\phi\frac{d\rho_g}{dt} \tag{9}$$

The gas is the only phase present in the reservoir, i.e., the crossing of the dew point line is not permitted to avoid condensate fallout in the pores. Fluid behaviour is governed by Black Oil fluid model.

$$\rho_g = \frac{\rho_{gs}}{B_g} = \frac{\text{constant}}{B_g} \tag{10}$$

The continuity equation is then written in terms of formation volume factor instead of density. Combining (9) with (7), we get the final diffusivity equation for one dimensional single-phase gas flow.

$$\frac{d^2P}{dx^2} \pm q_g = A_2\left(\frac{\mu}{K*b_g} + 2\beta v\right)\left(\frac{dP_g}{dt} + \frac{v}{\phi}\frac{dP}{dx}\right) \tag{11}$$

where $A2 = \phi\frac{db_g}{dP_g}$, $b_g = \frac{1}{B_g}$ (Inverse of formation volume factor, Bg ($\frac{\text{rcf}}{\text{scf}}$)); q_g represents source/sink term.

B. Matrix Region

For the matrix region, adsorbed gas is present in addition to free gas, which is not accounted for in (11). As per the flow model described earlier, the gas adsorbed to the sphere acts as a source to the pores space in the cube, thus it can be treated as an injection well. The injection of gas/gas desorption starts when the pressure in the reservoir reaches critical desorption pressure. Replacing source term in (11) with desorption term (5), we get the diffusivity equation for the matrix region.

$$\frac{d^2P}{dx^2} + V_L\rho_R\frac{P_L}{(P+P_L)^2}\frac{dP}{dt} = A_2\left(\frac{\mu_g}{k_x b_g} + 2\beta v_g\right)\left(\frac{dP_g}{dt} + \frac{v}{\phi}\frac{dP}{dx}\right) \tag{12}$$

C. Fracture Region

In the high permeable fracture zone, flow is assumed to be Darcy type in both directions x and z. The diffusivity equation in such case is given by:

$$\frac{\partial}{\partial x}\left(\frac{CK_x b_g}{\mu_g}\frac{\partial p_g}{\partial x}\right) + \frac{\partial}{\partial z}\left(\frac{CK_z b_g}{\mu_g}\frac{\partial p_g}{\partial z}\right) + q_{g\,(i,k)} = \emptyset\frac{db_g}{dp_g}\frac{\partial p_g}{\partial t} \tag{13}$$

D. Solution Procedure

The system is solved numerically by using Finite Difference Scheme. The discretization in time is done using implicit scheme for unconditional and stable solution. The gas is produced at constant bottom hole pressure. Let (i,k) denote grid cell number in 2D and t be the time step indices. First order derivatives have following forms:

$$\frac{dP}{dx} = \frac{P_{i,k+1}^{t+1} - P_{i,k}^{t+1}}{\Delta x} \tag{14}$$

$$\frac{dP}{dx} = \frac{\Delta x P_{i,k}^{+}}{\Delta x} \tag{15}$$

$$\frac{dP}{dt} = \frac{P_{i,k}^{t+1} - P_{i,k}^{t}}{\Delta t} \tag{16}$$

$$\frac{dP}{dt} = \frac{P_{i,k}(t+\Delta t) - P_{i,k}(t)}{\Delta t} \tag{17}$$

Second order derivatives have following forms:

$$\frac{d^2P}{dx^2} = \frac{P_{i,k+1}^{t+1} - 2P_{i,k}^{t+1} + P_{i,k-1}^{t+1}}{(\Delta x)^2} \tag{18}$$

$$\frac{d^2P}{dx^2} = \frac{P_{i,k+1}^{t+1} - P_{i,k}^{t+1} + P_{i,k-1}^{t+1} - P_{i,k}^{t+1}}{(\Delta x)^2} \quad (19)$$

$$\frac{d^2P}{dx^2} = \frac{\Delta x P_{i,k}^{+} + \Delta x P_{i,k}^{-}}{\Delta x^2} \quad (20)$$

where *dx, dz* represent derivatives in space and *dt* derivative in time. By introducing derivatives into (13), we get:

$$\left(\frac{Ckb}{A_2\mu + 2A_2\beta vkb}\right)\left(\frac{\Delta x P_{i,k}^{+} + \Delta x P_{i,k}^{-}}{\Delta x^2} + \frac{\Delta z P_{i,k}^{+} + \Delta z P_{i,k}^{-}}{\Delta z^2}\right) - \frac{v}{\phi}\left(\frac{\Delta x P_{i,k}^{+}}{\Delta x} + \frac{\Delta z P_{i,k}^{+}}{\Delta z}\right) = \frac{dP}{dt} \quad (21)$$

Multiplying both sides of the equation with A_2, we get:

$$\left(\frac{Ckb}{\mu + 2\beta vkb}\right)\left(\frac{\Delta x P_{i,k}^{+} + \Delta x P_{i,k}^{-}}{\Delta x^2} + \frac{\Delta z P_{i,k}^{+} + \Delta z P_{i,k}^{-}}{\Delta z^2}\right) - \frac{vA_2}{\phi}\left(\frac{\Delta x P_{i,k}^{+}}{\Delta x} + \frac{\Delta z P_{i,k}^{+}}{\Delta z}\right) = A_2\frac{dP}{dt} \quad (22)$$

We use 6x3 cells and 700-time steps to analyze production profiles. Fig. 4 gives the flowchart for the solution procedure used. A simulator is developed using a FORTRAN compiler to simulate the model results with user input parameters.

V. Analytical Fracture Model

We present an analytical fracture model for the flow of gas towards one single vertical fracture connected to a horizontal well. The derived equation shows a way to calculate pressure at any point in the vertical fracture. A rectangular fracture model (Fig. 5) is considered where the flow of fluid is according to the Darcy law. The inflow of fluid from the formation is linear. The pressures obtained in the fracture through analytical model is then compared with the numerical solution to study the stability and applicability of the numerical model.

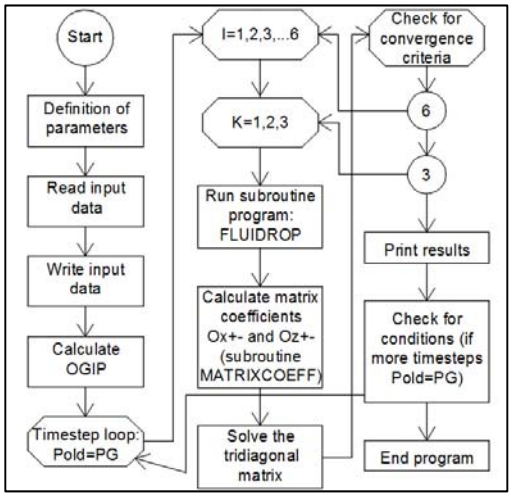

Fig. 4 Flowchart for programming on FORTRAN compiler

A. Linear Flow towards a Rectangular Fracture

Darcy's law gives us:

$$q = -\frac{K_m A}{\mu}\frac{\Delta p}{L} \quad (23)$$

For a rectangular fracture, A = h.ΔY

$$q = -\frac{K_m h\Delta Y}{\mu}\frac{dp}{dx} \quad (24)$$

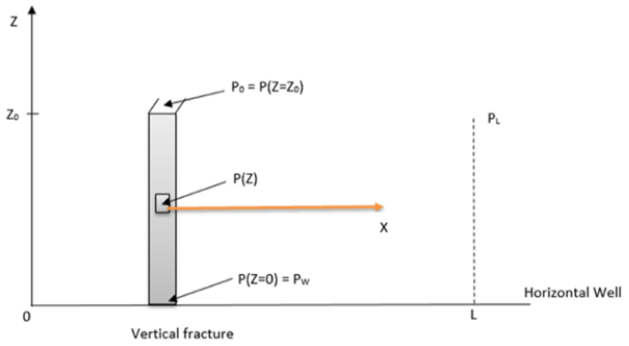

Fig. 5 Representation of fracture model used for analytical solution [3]

Rearranging and integrating, we get,

$$\int_{\Delta x}^{L} q\,dx = -\int_{p}^{p_e}\frac{K_m h\Delta Y}{\mu}\,dp$$

$$q = -\frac{K_m h\Delta Y(p_e - p)}{\mu(L - \Delta x)}$$

$$q(Z) = -\frac{(Z_0 - Z)\Delta Y K_m(p_e - p(z))}{\mu(L - \Delta x)} \quad (25)$$

Rearranging based on pressure difference instead of flow rate, we get,

$$p_e - p(z) = -\frac{q(Z)\mu(L - \Delta x)}{(Z_0 - Z)\Delta Y K_m} \quad (26)$$

At the top of the fracture, the length Z is equal to the fracture length Z_0. Thus from (25), we get,

$$For\ z = Z_0 \rightarrow\ q(Z_0) = 0 \quad (27)$$

This implies there will be no drainage at the top of the fracture. Similarly, at the bottom of the fracture, Z= 0, thus,

$$q(0) = -\frac{Z_0\Delta Y K_m(p_e - p(0))}{\mu(L - \Delta x)} \quad (28)$$

B. Linear Flow in the Fracture

Again, from Darcy's law, for the flow in fracture, we have:

$$q = -\frac{K_f A_f}{\mu}\frac{dp}{dz} \quad (29)$$

where A_f represents the cross-sectional area of the rectangular fracture.

$$A_f = \Delta x.\Delta y$$

$$q(Z) = -\frac{K_f \Delta x.\Delta y}{\mu}\frac{dp}{dz} \quad (30)$$

Since it is a connected system as per Fig. 5, we can equate (30) into (25), we get,

$$-\frac{(Z_0-Z)\Delta Y K_m(p_e-p(z))}{\mu(L-\Delta x)} = -\frac{K_f A_f}{\mu}\frac{dp}{dz}$$

Rearranging above equation, we get,

$$\frac{(Z_0-Z)(p_e-p(z))}{(L-\Delta x)}\frac{\Delta Y K_m}{K_f A_f} = \frac{dp}{dz} \quad (31)$$

Defining $a = \frac{\Delta Y K_m}{(L-\Delta x)K_f A_f}$ and substituting a in (31), we get,

$$a(Z_0 - Z)(p_e - p(z)) = \frac{dp}{dz}$$

$$\frac{dp}{(p_e-p(z))} = a(Z_0 - Z)dz$$

Integrating, we get,

$$-ln(p_e - p(z)) = a\left(Z_0 Z - \frac{1}{2}Z^2\right) + C \quad (32)$$

At $Z = Z_0$, pressure in the fracture is equal to well pressure, i.e. $p = p_w$. This implies, $-\ln(p_e - p_w) = C$. Substituting in (32), we get,

$$ln\left(\frac{p_e-p}{p_e-p_w}\right) = -a\left(Z_0 Z - \frac{1}{2}Z^2\right)$$

$$\left(\frac{p_e-p}{p_e-p_w}\right) = e^{-a\left(Z_0 Z-\frac{1}{2}Z^2\right)}$$

Resultant equation to calculate pressure at any height or point in the vertical fracture for linear inflow from the formation and linear flow in the fracture is then given as:

$$P_Z = P_e - (P_e - P_{well})\, e^{-a(z_0 z - 1/2\, z^2)} \quad (33)$$

where $a = \frac{\Delta Y K_m}{(L-\Delta X) K_f A_f}$; P_Z – Pressure at point Z along the fracture (psi); P_e – Reference pressure (psi); P_{well} – Well pressure (psi); z_0 – Total fracture length (ft); L – Linear extent of the reservoir (ft); K_m – Matrix permeability (mD); K_f – Fracture permeability (mD); A_f – Cross-sectional area of fracture (ft^2). The derivation of (33) is based on the model for radial in-flow of fluid [14]. This model has been modified for a linear inflow of fluid into a rectangular fracture.

VI. Results and Discussions

The following data (as shown in Table I) has been used in simulator. Data for Langmuir's isotherm are taken from Barnett Shale. Sensible and applicable data has been chosen to describe shale gas characteristics and reservoir properties [3].

A. Production Profile

On using the data from Table I and homogeneous reservoir property, we obtain the following production profile:

The production plot, Fig. 6, shows a long term well performance characteristics as desired in case of shale gas production. Here the initial reservoir pressure is 3100 psi and the gas is produced at constant bottom-hole pressure of 2550 psi. At an early stage of production, free gas present in the natural fracture and pore space is produced until the pressure in the cell reaches critical desorption pressure. The adsorbed gas then feeds the porous area through desorption at a rate dependent on pressure changes. However, a small bump or drop in the production rate is observed at around 200th time step in Fig. 6. This is because the free gas will be produced first from the cells closest to the fracture, thus the pressure in that cell will reach critical desorption pressure faster than other cells. As a result, the production rate stabilizes. After certain amount of time, when all the adsorbed gas has desorbed from the nearest cell to the well fracture, free gas will start coming out from the next adjacent cell until critical desorption pressure is reached, for adsorbed gas to be produced and stabilize the production rate again. Thus, we see a slight decrease in production rate when gas being produced moves from one cell to another [3].

TABLE I
Input Parameters Used for Simulation

Parameter	Value	Unit
Initial reservoir pressure	3100	psi
Gas viscosity	0.0184	cP
Gas formation volume factor (b_g)	1.35	scf/rcf
Initial dbg/dp, compressibility	6.30E-05	1/psi
Density of gas	6.42	lb/ft^3
Matrix permeability	0.001	mD
Porosity	0.05	fraction
Cell length	100	ft
Cell width	100	ft
Cell height	100	ft
Fracture length	20	ft
Fracture permeability	500	mD
Well radius	0.3	ft
Bottom-hole pressure	2550	psi
Perforation length	20	ft
Langmuir's volume	0.09914	scf/lb
Langmuir's pressure	2695.57	psi
Critical desorption pressure	2800	psi
Density of shale rock	168.55	lb/ft^3
Velocity	0.0001	m/s
Beta (non-Darcy constant)	0.00001	atm-sec^2/gm

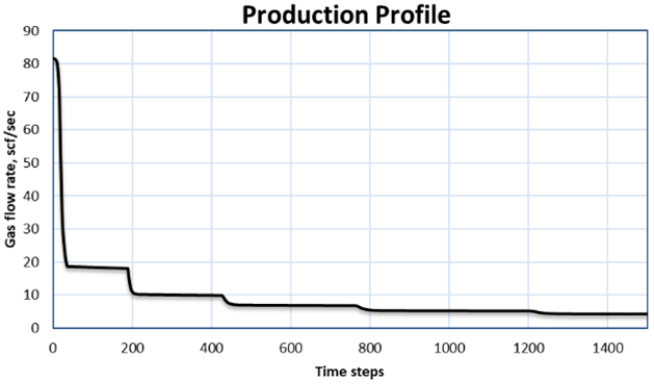

Fig. 6 Gas flow rate vs time steps

B. Pressure Variation in Individual Cells

Consider a 6x3 configuration of cells in 2D reservoir, as shown in Fig. 7. Fig. 8 indicates the individual cell pressures

in layer 1 of the shale formation. From the plot, we see that each cell will have its own independent behaviour with time.

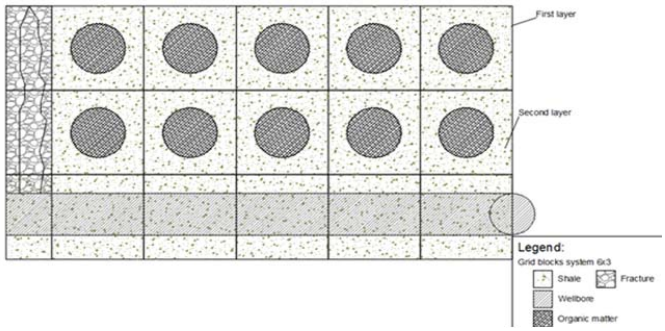

Fig. 7 Model system with 6x3 grid blocks

At an early stage of production free gas will be produced first and faster from the first block (1,2) which is closest to the fracture. Hence, pressure drop is much faster. After certain period, the pressure stabilizes which is due to desorption of gas as critical desorption pressure is reached. However, we see a continued drop in pressure in the remaining cells as it takes time for the gas to flow due to low matrix permeability.

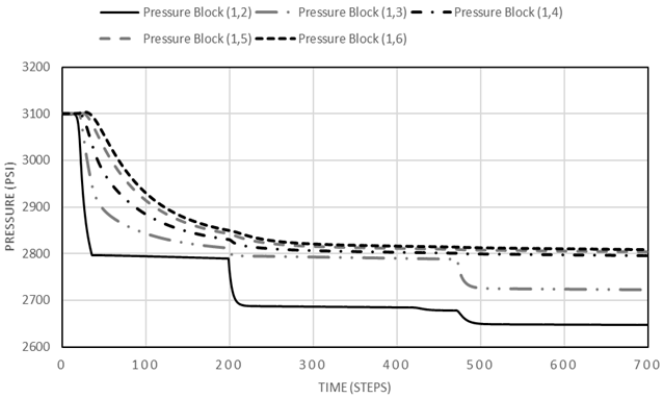

Fig. 8 Pressure variations in first layer of the system

Similar trend is seen for layer 2 of the reservoir. However, critical desorption pressure is reached faster than that in layer 1. One point to note is that the transmissibility of gas in z-direction within different layers is not considered. This assumption is acceptable because of low matrix permeability and thus the flow of gas will be towards fracture where pressure is low and not towards the adjacent cell in z-direction. Overall, the flow in z-direction is considered only in the fracture [3].

C. Volume of Desorbed Gas

Fig. 9 shows the volume of gas desorbed in each cell with time. The desorbed gas is produced first from the block (2,2) which is nearest to the vertical fracture and hence the pressure will be depleted faster. Desorption of gas will stabilize the pressure and flow rate until all the gas has been desorbed from that cell. Next, pressure in the adjacent will deplete and reach critical desorption pressure which will feed gas to the pore space. Such a trend will continue through the reservoir for a homogeneous system. For a heterogeneous system, we might observe some change in the order of desorption from the cell because of difference in porosity and permeability [3].

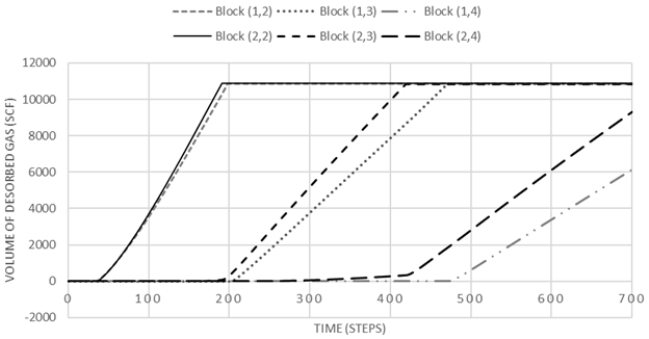

Fig. 9 Volume of desorbed gas for first three blocks in different layers

D. Effect of Forchheimer's Constant

In this section, we analyze the effect of β value (Forchheimer's constant [5]) on the production. Fig. 10 shows the comparison of production profiles at different β values.

The Fig. 10 suggests that inertial effect in the flow of gas increases with the increase in β- value. Also from the plot, it can be seen that as β tends to zero, the flow approaches Darcy's flow with no inertial effect. The plot also gives good indication as to why using non-Darcy flow mechanism becomes prominent in modelling of shale gas production.

Also, it is good to mention, that value of 1500 for beta is not realistic, but it is chosen only to show its impact on the production profile. In many papers (f. e. [13]), value of beta is assumed to be zero.

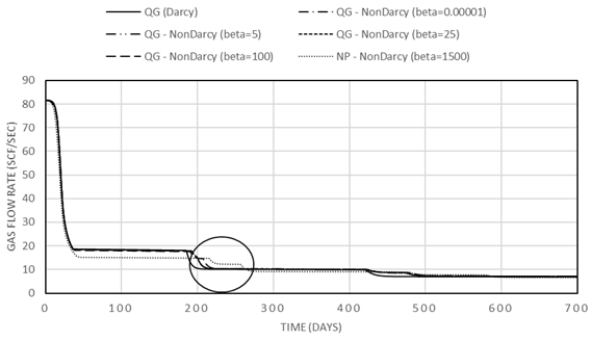

Fig. 10 Comparison of Darcy with non-Darcy flow at different β-value

E. Heterogeneous Reservoir Properties

Until now, the results shown are with homogeneous reservoir properties, i.e., with uniform permeability and porosity in each cell. In this section, we analyse the response of the model when heterogeneous properties are introduced to produce shale gas. This section also includes the comparison of production profile with varying size of the sphere or varying amount of adsorbed gas content. Also, we consider the implications of non-uniform fracture width.

Defining different porosity and permeability values to each

cell in the range of 0.5% to 7% and between 10^{-02} to 10^{-06} mD respectively. The plot obtained in Fig. 11 defines the stability and efficiency of the simulator developed.

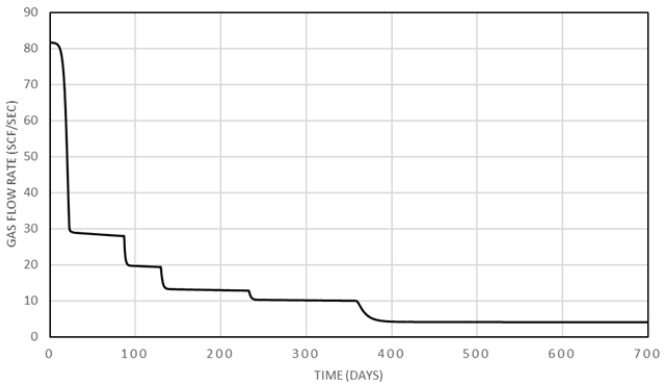

Fig. 11 Production profile for heterogeneous reservoir properties

F. Varying Size of Sphere

In this section, a comparison between production profiles for various sizes of sphere is made. Larger the size of sphere means higher the amount of organic content and the more amount of adsorbed gas. The comparison is made for three different radii of spheres: 15 ft, 20 ft and 40 ft. In addition, heterogeneous reservoir properties are used to obtain the production profile (Fig. 12).

The production for sphere of radius 40 ft sustains much longer at a good rate compared to spheres of radius 10 and 20 ft. This is because of the higher amount of gas content adsorbed due to presence of more organic matter. However, sphere with same size can also have different production profile if the adsorbed gas density is different. If a gas is much more densely packed or adhered onto the organic matter or has higher amount of total organic carbon (TOC) content, more gas is desorbed from that cell.

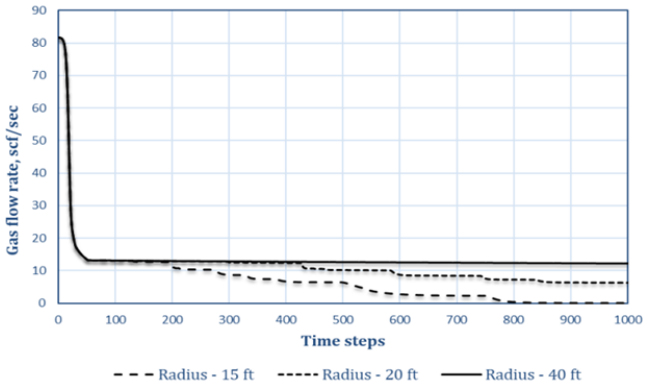

Fig. 12 Comparison between production profiles for 3 different sizes of sphere

Since the amount of gas adsorbed also depends on the density of gas, the following plot shows flow rate comparison between two different gas densities adsorbed onto the same size of sphere. We are now considering a sphere of radius 20 ft and gas densities of 6.42 lb/ft^3 and 15 lb/ft^3. The production will sustain longer in case of higher gas density because gas is more densely packed onto the organic matter and thus more amount of adsorbed gas. The overall Gas-in-place will also be larger with higher gas density. The obtained results are shown in Fig. 13.

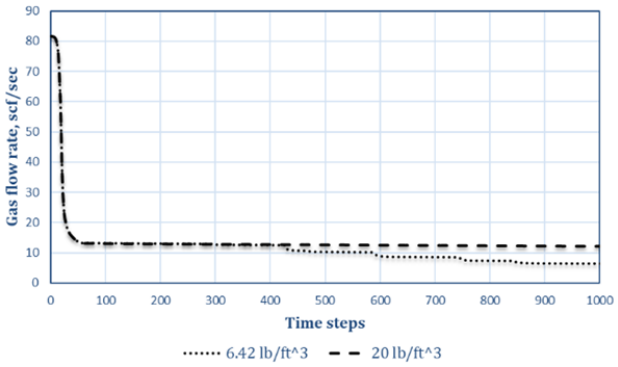

Fig. 13 Effect of Gas density on production profile

G. Varying Fracture Width

Until now, we had a uniform fracture width of 100 ft. Now in this section, we compare the production profile for a constant fracture width with non-uniform fracture width (Fig. 15). In the newly defined fracture, we are varying the width in the range of 20 ft to 60 ft as shown in Fig. 14.

For a uniform and constant fracture width, we see a low rate of production compared to non-uniform fracture width that is understandable as larger flow area is offered in case of non-uniform fracture width. The constant fracture width used is 20 ft. It would also be interesting to see how the pressure in grid blocks will behave with the change in fracture width. One such comparison is shown in Fig. 16 for block (2,3) at 2 different fracture widths of 20 ft and 40 ft.

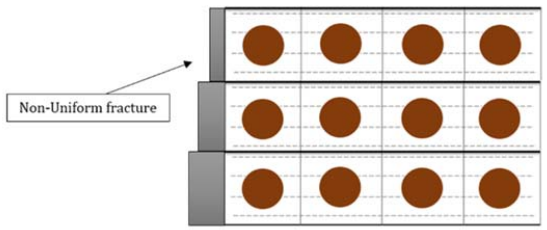

Fig. 14 Representation of non-uniform fracture width

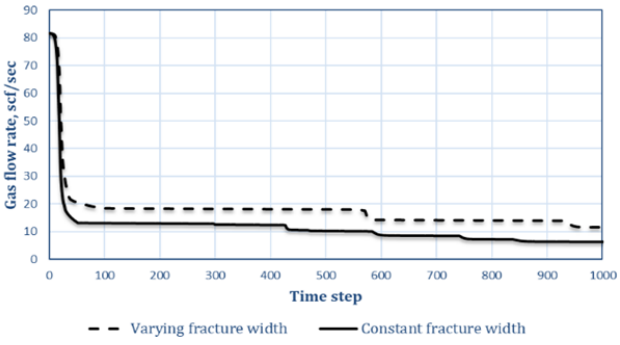

Fig. 15 Effect of fracture width on production profile

It shows that critical desorption pressure is reached at a later stage for fracture with width 40 ft compared to that of fracture with width 20 ft. In addition, the pressure in that block sustains for longer time. However, it is important to note that the plot shown is with heterogeneous reservoir properties, which will also influence the pressure variation in each block with time. Thus, it is difficult to predict how the pressure change will behave with facture width.

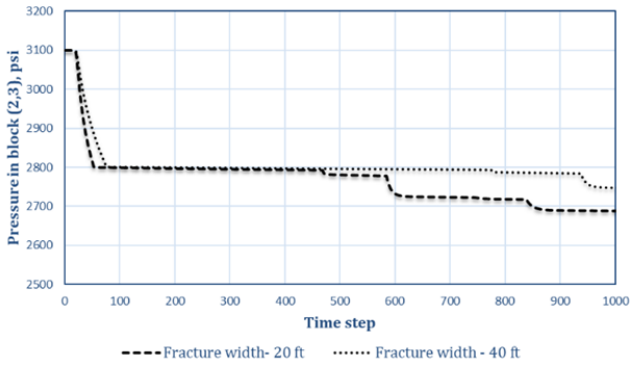

Fig. 16 Effect of varying fracture width on pressure in block (2,3)

Such more sensitivity analysis of the model for production of shale gas can be done with other parameters such as grid size, Langmuir's isotherm parameters and bottom-hole pressure and by producing gas at constant rate. However, results obtained by varying these parameters are not included in this paper.

H. Comparison-Analytical vs Numerical Solution

In Section V, we presented an analytical model to calculate pressure in a vertical rectangular shaped fracture. The analytical model considers linear inflow of fluid from the reservoir as well as linear flow in the fracture.

Fig. 17 shows the comparison between the pressures obtained through (5) with that of a numerical model. Pressure in the middle of fracture is compared with numerical solution, i.e., for analytical model, $Z = 150$ *ft.* and for numerical model, the centre point of block (2,1) is used.

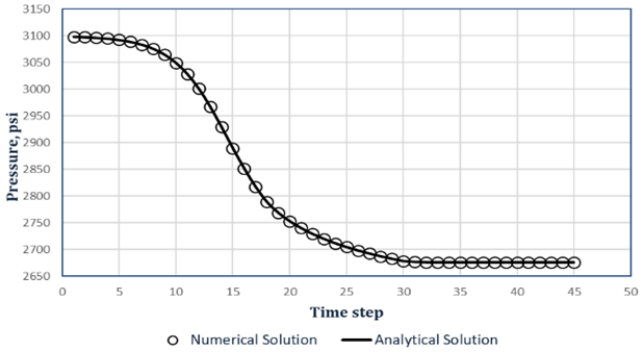

Fig. 17 Comparison between analytical and numerical fracture pressure

The fracture pressure obtained numerically gives a good match with the analytical model at various time steps. This shows the stability and applicability of the numerical model. However, one must note that Fig. 17 compares only the pressure in the vertical fracture. The analytical model shown in Section V is to calculate fracture pressure only. Derivation of an equation to calculate pressures analytically in the formation is much more complicated and is beyond the scope of this paper.

VII. Conclusions

A new flow model to produce shale gas is presented by localizing the presence of organic matter and inorganic matter within the shale to different places. The gas is stored through the means of compression as free gas and as an adsorbed gas onto the kerogen or organic matter. The transport mechanism considered are diffusion for the transport of gas within the matrix and the non-Darcy flow for the flow in micro-fractures and fractures created through stimulation job. However, for the time being, the transport of gas through diffusion is neglected, which will be considered in future work.

We discussed a shale gas flow model by considering a sphere inside a cube. The sphere comprises of organic matter where the transport of gas is through diffusion into the nanopores or matrix. Outside the sphere is the inorganic matter where we have linear Darcy flow of gas in the naturally occurring micro-fractures. The depletion of reservoir is pressure dependent for the production of free gas whereas inside the sphere it is both pressure dependent for desorption process and concentration dependent for diffusion. The flow model shows a simple yet applicable way of modelling gas production to depict the long-term well performance characteristics.

1) The production profile obtained shows long-term well performance characteristics as desired in case of shale gas production. The presence of additional gas source in terms of adsorbed gas stabilizes the production after an initial drop when pressure in the cell reaches critical desorption pressure.
2) The model developed generates pressure data for all the cells at each time steps. The resultant plot shows that each cell behaves independently. Desorption of gas is triggered first in the cell closest to vertical fracture. In addition, the pressure in the fracture is analyzed and it has similar trend as of production rate because the production is pressure dependent only.
3) Due to the presence of very low matrix permeability, gas velocity within the shale gas reservoir is generally high and non-linear fluid behavior becomes prominent. Comparison between Darcy and non-Darcy flow shows the inertial effects in the flow of gas, which increases with the increase in gas velocity.
4) The model is tested with heterogeneous inputs of permeability, porosity, and grid size. The results have been convincing showing that model is able to handle variable inputs and efficient in forecasting production of shale gas. Moreover, the simulator is also able to non-uniform fracture width as an input.
5) Larger the size of sphere depicts more amount of gas

adsorbed or stored in the sphere. Moreover, the same size of sphere can have different quantity of gas adsorbed if the gas present is of different liquid like densities.

6) The analytical model shows an efficient way of calculating pressures and flow rate at any point in the fracture depending on the well pressure.
7) The pressures obtained analytically in the fracture are compared with the numerical solution for a given well pressure. The result shows a good match between the two models. This also implies the applicability, stability and efficiency of our numerical model.

REFERENCES

[1] Alexander, T., Baihly, J., Boyer, C., Clark, B., Waters, G., Jochen, V.... . Toelle, B. 2011. Shale Gas Revolution. *Oilfield Review Autumn*, Schlumberger, pp. 40-41.
[2] Javadpour, F., Fisher, D., Unsworth, M., 2007. Nanoscale gas flow in shale gas sediments. Journal of Canadian Petroleum Technology, 46 (10).
[3] Berawala, D. 2015. Modelling of Gas Production from Tight Shale Formations: An Innovative Approach (Master Thesis, University of Stavanger, Norway). Retrieved from https://brage.bibsys.no/xmlui/handle/11250/301296
[4] Langmuir, I., 1916. The constitution and fundamental properties of solids and liquids. Journal of the American Chemical Society, 38 (11): 2221–2295.
[5] Forchheimer, P., 1901. Wasserbewgung durch Bodenl. Zeitschirift des Vereines Deutscher Ingenieuer, 45 edition.
[6] Grathwohl, P. 2006. Diffusion II, HGC II. Retrieved from http://www.uni-tuebingen.de/zag/teaching/HGC/DiffusionII_2006.pdfJ.
[7] Moghanloo, R. G., Javadpour, F., & Davudov, D. 2013. Contribution of Methane Molecular Diffusion in Kerogen to Gas-in-Place and Production. Paper SPE 165376 presented at the SPE Western Regional & AAPG Pacific Section Meeting, Joint Technical Conferene, Monterey, California, USA, 19-25 April.
[8] Wang, C. 2013. Pressure Transient Analysis of Fractured Wells in Shale Reservoirs. Master Thesis. Colorado School of Mines. Colorado.
[9] Shi, J. and Durucan, S. 2005. Gas Storage and Flow in Coalbed Reservoirs: Implementation of a Bidisperse Pore Model for Gas Diffusion in a Coal matrix. SPE Reservoir Evaluation & Engineering Journal 8(2): 169-175. Paper SPE 84342-PA. doi: 10.2118/84342-PA.
[10] Swami, V., Settari, A., Javadpour, F. 2013. A Numerical Model for Multi-Mechanism Flow in Shale Gas Reservoirs with Application to Laboratory Scale Testing. Paper SPE 164840 presented at the EAGE Annual Conference & Exhibition incorporating SPE Europec, London, UK, 10-13 June.
[11] Firoozabadi A. 2012. Nano-Particles and Nano-Pores in Hydrocarbon Energy Production. Research talk delivered at University of Calgary, Dec 7.
[12] Loucks, R. G., Reed, R., Ruppel, S., Jarvie, D. 2009. Morphology, Genesis, and Distribution of Nanometer-Scale Pores in Siliceous Mudstones of the Mississippian Barnett Shale. Journal of Sedimentary Research, v. 79, 848-861.
[13] Nobakht, M., Clarkson, C., Kaviani, D. 2011. New and Improved Methods for Performing Rate-Transient Analysis of Shale Gas Reservoirs. Paper SPE 147869-MS presented at SPE Asia Pacific Oil and Gas Conference and Exhibition, Jakarta, Indonesia, 20-22 September.
[14] Espevold, I., Skoglund, L.K. 2013. Shale Gas Production – fluid flow towards wellbore. Bachelor Thesis. I. Espevold, L.K. Skoglung. Stavanger.